THE JOURNAL OF PHYSICAL CHEMISTRY C

Article

Band Edge Recombination in CdSe, CdS and CdSSe Alloy Nanocrystals Observed by Ultrafast Fluorescence Upconversion: The Effect of Surface Trap States

Maria Danielle Garrett, Albert D. Dukes III, James R. McBride, Nathanael J. Smith, Stephen J. Pennycook, and Sandra J. Rosenthal

J. Phys. Chem. C, **2008**, 112 (33), 12736-12746• DOI: 10.1021/jp803708r • Publication Date (Web): 23 July 2008

Band Edge Recombination in CdSe, CdS and CdS_xSe_{1-x} Alloy Nanocrystals Observed by Ultrafast Fluorescence Upconversion: The Effect of Surface Trap States

Maria Danielle Garrett,[†] Albert D. Dukes III,[†] James R. McBride,[†] Nathanael J. Smith,[†] Stephen J. Pennycook,[‡] and Sandra J. Rosenthal*[,†,§]

Department of Chemistry, Vanderbilt University, 7330 Stevenson Center, Station B 351822, Nashville, Tennessee 37235, Oak Ridge National Laboratory, Condensed Matter Sciences Division, Oak Ridge, Tennessee 37831, and Department of Physics and Astronomy, Vanderbilt University, 6301 Stevenson Center, 1807 Station B, Nashville, Tennessee 37235

Received: April 24, 2008; Revised Manuscript Received: June 12, 2008

The effect of surface trap states on band edge recombination in CdSe, CdS and CdS_xSe_{1-x} alloy nanocrystals has been determined using fluorescence upconversion spectroscopy. These measurements reveal that there is both a size and composition dependence on the short-lived (τ_1) and long-lived (τ_2) components of fluorescence lifetime at the band edge. An increase in nanocrystal diameter, ranging from 23 to 60 Å, is accompanied by an increase in τ_1. This behavior is explained by the decrease in accessible trap sites through a reduction in surface-to-volume ratio. Similarly, τ_2 is found to increase with increasing nanocrystal size. However, with increasing sulfur concentration in the alloy nanocrystals, both a reduction in the magnitude of τ_1 and a reversal in the trend for τ_2 are observed. These changes in lifetimes associated with the addition of sulfur are explained by increased trapping on the nanocrystal surface. These results indicate that carrier dynamics may be controlled not only through size, but also through composition of the nanocrystals. Compositional variation has been shown not only to affect carrier dynamics, but also to affect the optical properties of nanocrystals. An increase in the Stokes shift is observed for CdS_xSe_{1-x} alloy nanocrystals as compared to CdSe and CdS nanocrystals. This indicates that the Stokes shift is highly influenced by the nonlinear effects of alloying.

Introduction

The unique size-dependent optical and electronic properties[1–3] of semiconductor nanocrystals are important from both a fundamental and an applied perspective. While size-dependent tunability makes these materials ideal for applications such as photovoltaics, light-emitting diodes and biological labeling,[4–11] alloy nanocrystals offer the added advantage of composition-dependent tunability.[12] In particular, CdS_xSe_{1-x} alloy nanocrystals, spanning the compositional range from pure CdS ($x = 1$) to pure CdSe ($x = 0$), have band gap energies ranging from the UV to the visible. This makes CdS_xSe_{1-x} a potentially favorable material for biological imaging applications, where nanocrystals of the same size but with varying optical properties might be advantageous. Additionally, alloys provide easier access to difficult wavelengths. For example, a small red-emitting nanocrystal[13] would be useful for increased light penetration through the skin. A more intimate understanding of the dynamics of the CdS_xSe_{1-x} nanocrystals is needed in order for parameters to be specifically tailored for each individual application, making CdS_xSe_{1-x} an ideal material with which to study the compositional dependence of electron−hole recombination at the band edge.

Given that the kinetics of the photogenerated electron−hole pair in the nanocrystal defines the operational parameters for practical applications, an understanding of the behavior of the electron−hole pair is a necessity. As the synthetic methodologies of the nanocrystals continue to evolve, it is imperative to explore possible changes in the kinetics of the carrier dynamics of the nanocrystals resulting from changes in composition. Two extensive studies on the dynamics of bulk CdS_xSe_{1-x} were conducted by Gadd[14] and Hane.[15,16] Gadd performed time correlated single photon counting (TCSPC) and fluorescence upconversion experiments on bulk CdS_xSe_{1-x} ($x = 0.00$, 0.25, 0.50, 0.75 and 1.00 for TCSPC and $x = 0.00$, 0.25 and 0.50 for fluorescence upconversion). Using TCSPC, the measured lifetimes were found to be approximately 30 ps for all samples and, thus, were independent of composition. However, the fluorescence upconversion results showed much longer lifetimes, on the order of several hundred ps, that varied with composition. Hane also used TCSPC to study both graded and homogeneous CdS_xSe_{1-x} alloys. From this study it was found that for graded alloys, there is a strong dependence of the luminescence lifetimes on detection wavelength. From 500−620 nm, for CdSe/S graded alloys, longer lifetimes were exhibited at longer wavelengths. However, from 620−720 nm, shorter lifetimes were seen at longer wavelengths. In contrast, for CdS/Se graded alloys, the opposite trend was seen for comparable ranges of wavelengths. With homogeneous alloys, a strong lifetime dependence with changing composition was seen. While individual lifetimes were not reported, the lifetimes for the homogeneous alloys ranged from approximately 100−250 ps. The decays for CdSe and CdS were found to be equivalently fast. For alloys $x = 0.25$ and 0.75, the decays were intermediate, while $x = 0.50$ produced the longest decay.

While ultrafast studies have been conducted on bulk CdS_xSe_{1-x} alloys,[14–16] there has been no major focus on their nanocrystal counterpart. Most of the ultrafast studies on CdS_xSe_{1-x} alloy nanocrystals thus far have focused on nano-

* To whom correspondence should be addressed. E-mail: sandra.j.rosenthal@vanderbilt.edu.
† Department of Chemistry, Vanderbilt University.
‡ Oak Ridge National Laboratory.
§ Department of Physics and Astronomy, Vanderbilt University.

10.1021/jp803708r CCC: $40.75
Published on Web 07/23/2008

crystal doped glasses.[17–21] Zhang et al. studied the multiexciton recombination of CdS_xSe_{1-x} nanocrystal doped glasses using femtosecond transient absorption spectroscopy.[17] Of the two sizes examined, the 2.8 nm sample was found to have a risetime on the order of 200 fs, corresponding to the pulse width of the experiment. The second sample (2.6 nm) had a risetime slightly longer than the pulse width, indicating the excited-state relaxed into a state with a higher cross section for the probe pulse. Both sets of rise times were found to be independent of pump power. However, the decay time constants were found to decrease with increasing pump power as a result of high order exciton recombination. This behavior was attributed to both second-order exciton−exciton annihilation and Auger recombination, where increasing the pump power increases the concentration of charge carriers and, thus, the probability of electron−hole recombination.[17] Zhang and Izutsu also observed a relaxation time of approximately 2 ps for excited carriers in dangling-bond states for CdS_xSe_{1-x}-doped glasses, using femtosecond pump−probe experiments.[18]

Shen et al. studied the relaxation of photoexcited carriers through different channels for CdS_xSe_{1-x} nanocrystal doped glasses using the femtosecond ultrafast transient lensing technique.[19] They fit their data to three decay time constants for the samples. These three decays were attributed to direct recombination, excited-state trapping and trapping processes at the nanocrystal-glass interfaces. It was found, in CdS_xSe_{1-x} nanocrystals doped in glass, that there is an increase in the radiative decay rate as the nanocrystal sizes decreases.[19] Toyoda and Shen also used photoacoustic spectroscopy to study the CdS_xSe_{1-x} ($x = 0.26$) nanocrystals in a glass matrix.[20] They found this material exhibited triexponential behavior corresponding to direct recombination processes with possible trapping, and radiative and nonradiative recombination processes.

In this paper, we use femtosecond fluorescence upconversion to directly probe the depopulation of the excited-state in CdSe, CdS and CdS_xSe_{1-x} alloy nanocrystals. Although upconversion observes only the radiative recombination, a nonradiative process is also reflected in the decay. By varying the amount of sulfur and selenium in the alloy nanocrystals, we explore the composition dependence of electron−hole recombination at the band edge for CdS_xSe_{1-x} alloy nanocrystals in solution. These results reveal both a size and composition dependence on the short-lived (τ_1) and long-lived (τ_2) lifetime components and are compared to previously published fluorescence upconversion data on the dynamics of CdS_xSe_{1-x} bulk alloys. This work is critical in developing a better understanding of the strong effect that compositional variations have on surface trapping and band edge recombination.

Experimental Methods

CdSe, CdS and CdS_xSe_{1-x} Synthesis. Homogeneous alloy nanocrystals were synthesized as previously described by Swafford et al.[12] The synthesis was carried out in a single three-neck flask. The Cd precursor was prepared by combining 0.256 g of CdO (Puratrem, 99.999%), 2.4 mL of oleic acid (OA, Aldrich, 90%) and 10 mL of 1-octadecene (ODE, Aldrich, 90%). This solution was heated to 310 °C. The system was purged with argon until 140 °C. When the temperature reached 310 °C, a selenium:tributylphosphine (Strem, Se, 200 mesh and TBP, 97%) injection solution [15 mL of 0.1 M Se:TBP:ODE (diluted with ODE from a 4 M Se:TBP stock solution) for CdSe nanocrystals, 10 mL of 0.1 M S:ODE for CdS nanocrystals, or $10x$ mL of 0.1 M S:ODE with $10(1-x)$ mL of 0.1 M Se:TBP:ODE for CdS_xSe_{1-x} alloy nanocrystals] was swiftly injected and the temperature was reduced to 275 °C.

To grow nanocrystals larger than approximately 36 Å in diameter, it was necessary to add growth solution to the reaction flask. The growth solution was prepared by stirring 0.76 g of CdO, 6 mL of OA and 25 mL of ODE while heating to 290 °C. Once the solution reached temperature and turned clear, it was cooled to 50−100 °C while stirring. After reaching this temperature, $0.16x$ g of S powder was added and dissolved while stirring. This solution was then allowed to cool to room temperature. Upon reaching room temperature, $1.25(1-x)$ mL of a 4 M Se:TBP solution was added to the solution. The growth solution was then stirred until use. Growth solution was added to the initial reaction solution, immediately after the injection solution, at a rate of approximately 0.45 mL/min, until the nanocrystals reached the desired size.

Isolation of the nanocrystals was carried out by precipitation in a butanol:ethanol (1:4) mix, followed by centrifugation. The supernate was discarded, and the resulting solid was slurried in 5 mL of chloroform. The nanocrystals were then precipitated out of the chloroform by the addition of acetone and isolated by centrifugation.[22] The supernate was decanted from the pelleted solid and the nanocrystals were once again precipitated with the chloroform:acetone mix, followed by centrifugation. After disposing of the supernate, the solid nanocrystals were solvated in toluene or in hexanes.

Femtosecond Fluorescence Upconversion. Fluorescence upconversion spectroscopy was performed with a Coherent Verdi V18 (CW, 532 nm, 18W) that was used to pump a mode-locked Ti:Sapphire oscillator (Mira 900 Basic, Coherent). The output from the Mira was used to seed a regenerative amplifier (RegA 9000, Coherent), which in turn powered an optical parametric amplifier (OPA 9400, Coherent), from which the excitation and gate sources were obtained. Operating at a repetition rate of 250 kHz, the system produced pulses typically ranging from 150−200 fs (fwhm) leading to instrument response functions spanning approximately 200−280 fs (fwhm). For CdSe, the tunable, visible OPA output (480−750 nm) was used as the sample excitation source. In order to minimize the effect of the instrument response function on the spectrum, the OPA was tuned 20 nm above the band edge absorption of the CdSe nanocrystals. The frequency-doubled fundamental (400 nm) was selected as the pump source for the CdS and CdS_xSe_{1-x} nanocrystals due to their lower wavelength band edge absorption and the limitations of the tunable OPA output. Additional samples of OA synthesized CdSe were also excited at 400 nm to check the effect of excitation wavelength on the dynamics. The residual 800 nm light remaining from the doubling process in the OPA was used as the gate beam.

For excitation 20 nm above the band gap, samples were allowed to flow in anhydrous toluene through a 2 mm quartz cell under argon or nitrogen and excited by the focused tunable beam. However, because of interference with the upconverted signal due to the UV cutoff for toluene, hexanes were used for samples excited at 400 nm. A rhodium coated elliptical reflector focused the sample emission onto a nonlinear mixing crystal (1 mm XC8-$LiIO_3$-Type I SFM-800/500−1000//308−444 nm, Cleveland Crystals, Inc.). The upconverted signal was maximized by a suitable choice of the angle of the nonlinear mixing crystal. For excitation at 400 nm, a color glass filter (03FCG579, Melles Griot) was used to filter out residual excitation light.

A UV-dispersing prism (STS#37261, CVI Laser Corp.) was used to separate the upconverted signal from any residual light. The upconverted signal was then directed into a UV-optimized

monochromator (McPherson), detected by a photon-counting photomultiplier tube (R1527P, Hamamatsu) and digitized with a photon counter (SR400, Stanford Research Systems). The fitting function used to analyze the data was derived from the convolution of the Gaussian laser pulse with a decaying exponential:[23]

$$F(t,A,\tau,W)=\frac{A}{2}\left[1+erf\left(\frac{1}{4}\right)\left[\frac{8t\ln 2-\frac{W^2}{\tau}}{W\sqrt{\ln 2}}\right]\right]\times \exp\left[\frac{-\left(\frac{(16t\ln 2)}{\tau}-\frac{W^2}{\tau^2}\right)}{16\ln 2}\right] \quad (1)$$

where A is amplitude of the decay, W is the fwhm of the Gaussian, and τ is the decay time constant. To allow the position of the Gaussian to "float" relative to the exponentials, a time shift (t_0) was added to the fitting function. Additionally, an offset was added so that the exponential decays back to the baseline rather than to zero. In order to account for multiple electron−hole recombination pathways, conventionally, several decays are used for fitting ultrafast data.[1,23–26] The fitting function is the summation of as many convolved functions as observed decay processes

$$\sum_{i=0}^{n}\frac{A_i}{2}\left[1+erf\left(\frac{1}{4}\right)\left[\frac{8(t-t_0)\ln 2-\frac{W^2}{\tau_i}}{W\sqrt{\ln 2}}\right]\right]\times \exp\left[\frac{-\left(\frac{(16(t-t_0)\ln 2)}{\tau_i}-\frac{W^2}{\tau_i^2}\right)}{16\ln 2}\right]+offset \quad (2)$$

For the data presented here, two lifetimes were observed: a short-lived (τ_1) and long-lived (τ_2) decay. Additionally, for several samples, a risetime (τ_3) was observed.

Results and Discussion

Characterization. The band edge absorption wavelength (Figure 1a−e) of each sample was measured using a Varian Cary 50 UV−vis spectrophotometer. The typical nanocrystal size dependence of the band gap is apparent in Figure 1a−d; while Figure 1e reveals the composition dependence of the band gap. Each sample was excited at either 20 nm above the band edge absorption or at 400 nm, and the fluorescence upconversion data was collected at the peak wavelength of the static emission spectrum (Figure 1f). A compositional dependence of the Stokes shift is observed for CdSe, CdS and CdS_xSe_{1-x} alloy nanocrystals. Although the nonresonant Stokes shift is known to decrease with increasing nanocrystal size,[27] based on such previous reports in literature, the Stokes shift for the size range examined in this work is relatively constant.

The nonresonant Stokes shift is tied to the band-edge exciton fine structure, where the nonresonant Stokes shift is the energy difference between the two upper states of the band-edge exciton fine structure and the dark exciton ground state.[27,28] The nonresonant Stokes shift may also be influenced by dispersions in shape, inhomogeneity in structure, and phonon effects.[27,28] While only a small Stokes shift[1,29] is observed for CdSe and CdS, the Stokes shift almost doubles for CdS_xSe_{1-x} alloy nanocrystals (Figure 2a). Similarly, increases in Stokes shift with changing alloy composition have previously been seen in

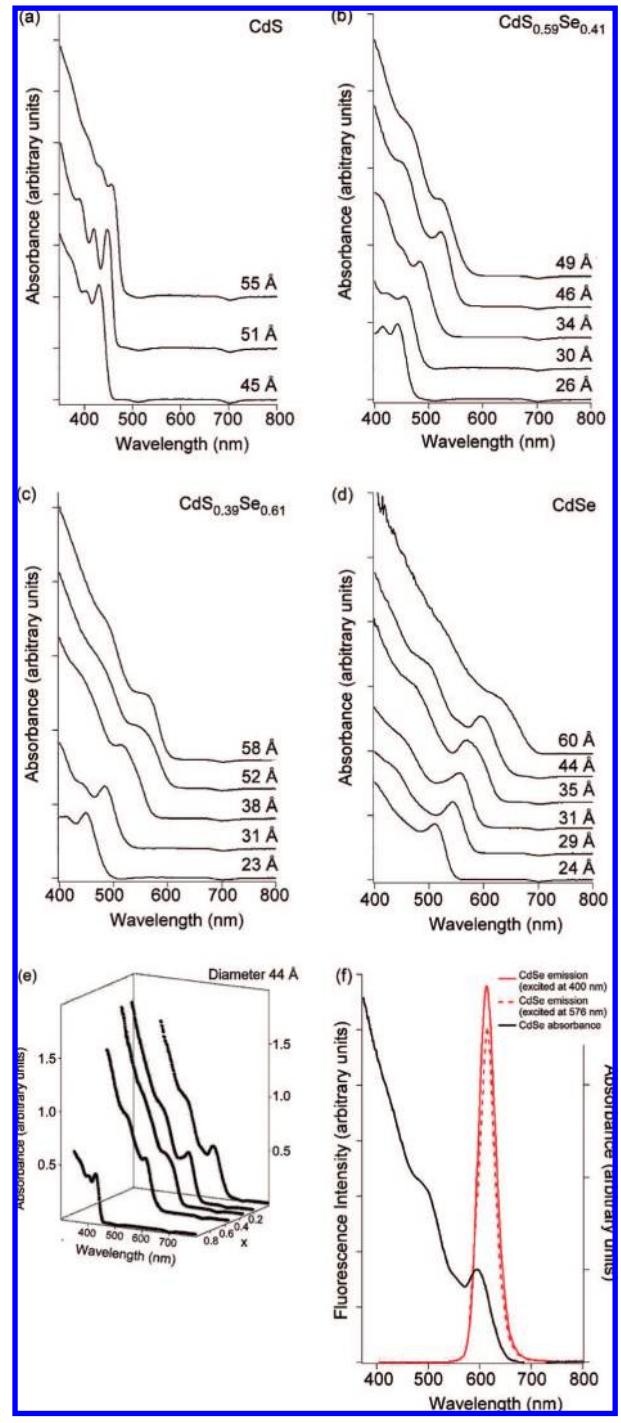

Figure 1. Absorbance spectra for (a) CdS nanocrystals ranging in size from 45 to 55 Å, (b) $CdS_{0.59}Se_{0.41}$ alloy nanocrystals ranging in size from 26 to 49 Å, (c) $CdS_{0.39}Se_{0.61}$ alloy nanocrystals ranging in size from 23 − 58 Å, (d) CdSe nanocrystals ranging in size from 24 to 60 Å, (e) 44 Å (±5%) nanocrystals spanning the compositional range from pure CdS ($x = 1$) to pure CdSe ($x = 0$), and (f) representative absorption and emission spectra for CdSe nanocrystals. To run the fluorescence upconversion experiment, CdSe samples were typically excited 20 nm above the band edge, while CdS and CdS_xSe_{1-x} samples were excited at 400 nm. Additional samples of CdSe were excited at 400 nm to check the effect of excitation wavelength on electron−hole recombination at the band edge.

$In_xGa_{1-x}N$[30] and $Zn_{1-x}Cd_xO$[31] alloy films, and, most notably, in $CdSe_{1-x}Te_x$ alloy nanocrystals.[32]

Bailey and Nie[32] observe a nonlinear relationship between alloy composition and the band gap peak absorption and emission for $CdSe_{1-x}Te_x$ alloy nanocrystals. They attribute the

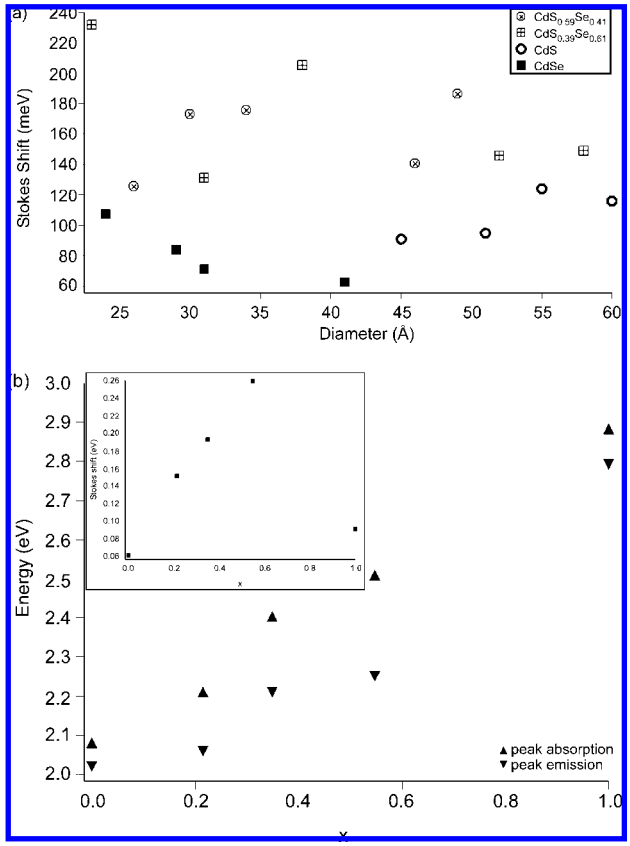

Figure 2. Graph of (a) Stokes shift (meV) versus nanocrystal size for different alloy compositions and (b) peak absorption and emission (eV) for 44 Å (±5%) nanocrystals spanning the compositional range from pure CdS ($x = 1$) to pure CdSe ($x = 0$), where the change in Stokes shift with composition is nonlinear. The inset depicts the Stokes shift (eV) for the 44 Å alloy nanocrystal series.

exceptionally large Stokes shift to nonlinear effects, such as optical bowing. Although the bowing parameter, a measure of the degree of nonlinearity, for CdS_xSe_{1-x} is smaller than for $CdSe_{1-x}Te_x$, [12,33] the change in Stokes shift with composition is clearly nonlinear (Figure 2b) for CdS_xSe_{1-x} alloy nanocrystals. Such nonlinear effects can be attributed to changes in the band structure due to variations in the lattice constant, deformation of the electron distribution due to different electronegativity values of the ions in the alloy, and structural ordering of different sized ions due to relaxation of anion−cation bonds.[12,32] Not only does the Stokes shift increase significantly for CdS_xSe_{1-x} alloy nanocrystals, but it also appears to reach a maximum value near the middle of the compositional range (inset Figure 2b). Similar behavior has been reported for $In_{1-x}Ga_xN$ alloys.[34] Wu et al. attribute this behavior to a nonuniform distribution of the cations, implying that compositional variation or structural disorder is maximized near the middle of the compositional range. Their reasoning also coincides with Hane's work on CdS_xSe_{1-x} bulk alloys, which states that maximized localization may well be near $x = 0.50$, where the material is most disordered.[16]

The synthesized nanocrystals were found to be highly crystalline and have a zinc-blende structure.[12] High resolution transmission electron microscopy (HRTEM) images were taken to check the size and to ensure each alloy sample consisted of monodisperse nanocrystals (Figure 3). Atomic number contrast scanning transmission electron microscopy (Z-STEM) was used to obtain spatially resolved chemical information about the nanocrystals.[35,36] As heavier elements scatter electrons more effectively, they appear brighter in Z-STEM images. Thus, core/shell structures exhibit a distinct difference in intensity between the core and shell materials. In contrast, homogeneous alloy nanocrystals should appear uniformly bright. As seen in Figure 4, our materials are uniform in intensity, confirming that we have synthesized homogeneous alloy nanocrystals.

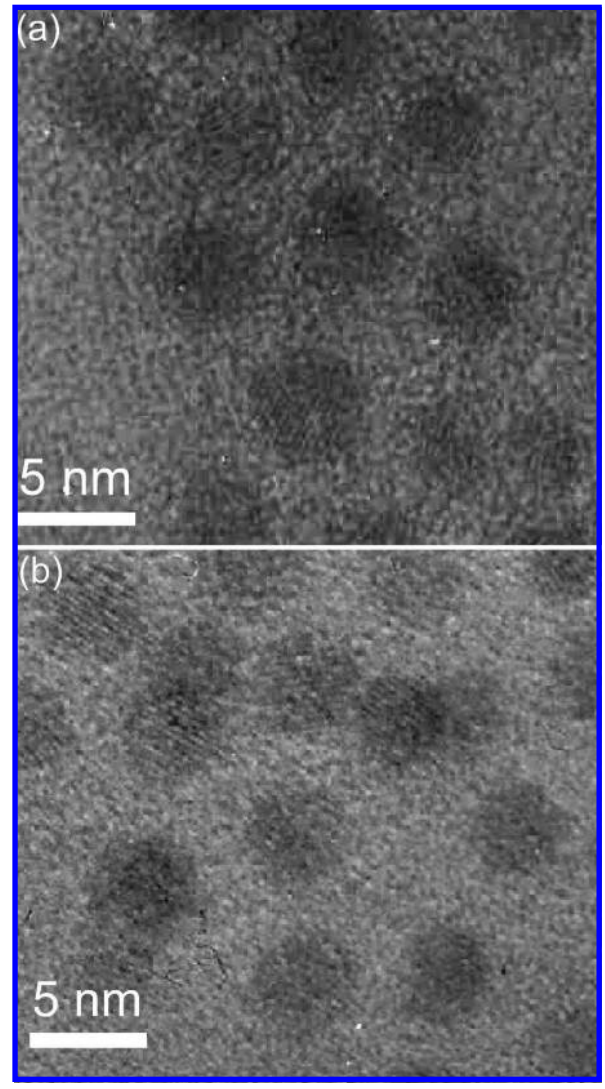

Figure 3. (a) HRTEM images of $CdS_{0.38}Se_{0.62}$ 52 Å alloy nanocrystals and (b) $CdS_{0.58}Se_{0.42}$ 49 Å alloy nanocrystals.

Homogeneity of the CdS_xSe_{1-x} alloy nanocrystals has been previously verified in the literature. Swafford et al. conducted an extensive Rutherford backscattering spectroscopy (RBS) study where it was found that the composition of CdS_xSe_{1-x} was nearly constant over the entire growth period, indicating a homogeneous alloy rather than a core/shell structure.[12] In order to verify the composition of the material being used for the fluorescence upconversion experiments presented in this work, RBS was used to determine the compositional ratio of each sample (Figure 5a). For a given composition series, the composition distribution of each alloy nanocrystal sample falls within ± 5% (Figure 5b).

Carrier Dynamics. The fluorescence lifetime data for CdSe, CdS and CdS_xSe_{1-x} alloy nanocrystals ranging in size from 23 to 60 Å, collected using ultrafast fluorescence upconversion, are shown in Figure 6. For most of these samples, three lifetimes were observed: a short-lived (τ_1) and long-lived (τ_2) decay and a risetime (τ_3). The corresponding amplitude percentages extracted from the fits for each decay lifetime are given in Tables

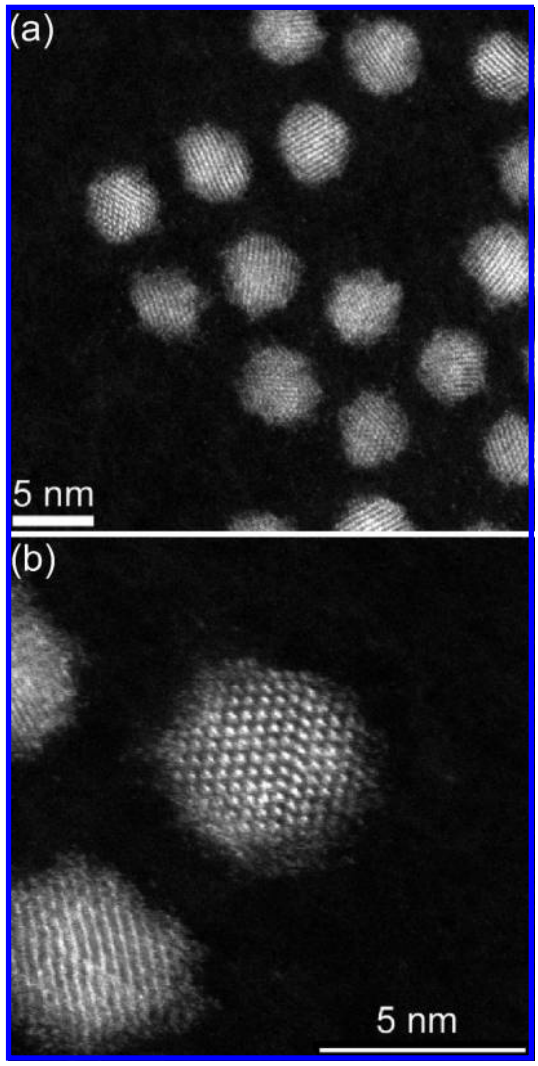

Figure 4. (a) Z-STEM image of $CdS_{0.50}Se_{0.50}$ 51 Å alloy nanocrystals taken on a VG Microscopes' model HB603U, operating at 300 kV and fitted with a Cs corrector from Nion, located at Oak Ridge National Laboratory. The operation and data collection were done with Digital Micrograph. (b) It can be seen that there is no core/shell structure, as the nanocrystal is uniform in intensity.

1 and 2. It should be mentioned again that although the excitation source was tuned to 20 nm above the band edge absorption of the OA synthesized CdSe nanocrystals, a 400 nm excitation source was used for the CdS and CdS_xSe_{1-x} nanocrystals.

Pumping the system at energies greater than twice the band gap of the semiconductor nanocrystal results in the generation of multiexcitons.[37] By probing the intraband transitions in the mid-IR, Ellingson et al. found that the exciton decay observed with an increase in photon energy is related to nonradiative recombination of multiexcitons through Auger recombination.[37] While initial measurements of the risetime of the transient absorption data did not indicate any sign of carrier multiplication, analysis of the decay data for inter- and intraband transient absorption indicated that the biexciton effect, while important in the first few ps, does not influence the long-term decay dynamics.

Seeing that the excitation source was never double the band gap of any sample presented in this work, carrier multiplication was not a concern. However, additional samples of CdSe were also excited at 400 nm to verify that there was no significant

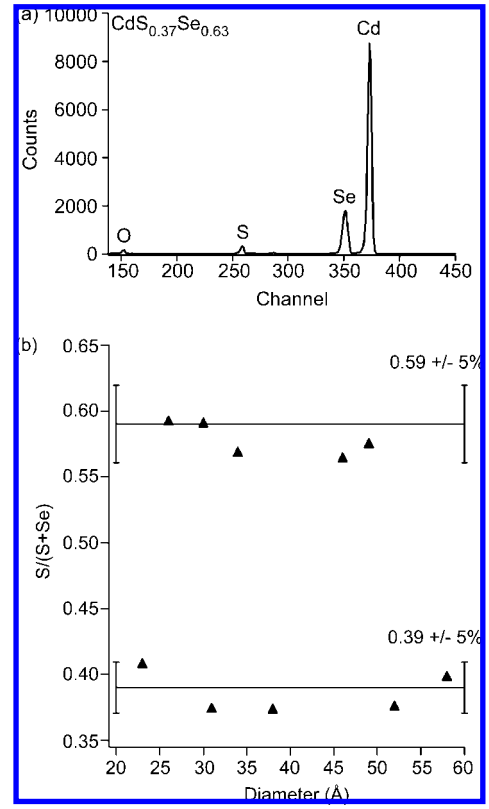

Figure 5. (a) Representative RBS spectrum of CdS_xSe_{1-x} alloy nanocrystals and (b) compositional ratios, S/(S+Se), determined from RBS measurements. For a given composition series, the composition distribution of each alloy nanocrystal sample falls within ±5%.

effect of excitation wavelength on the dynamics. Although it has been reported that increasing the excitation energy may produce more relaxation pathways, involving surface or external energy states, that reduce the efficiency of charge carrier relaxation to the band edge,[38] this does not appear to have a critical effect on the trends we report here. As seen in Figure 7, there is no appreciable dependence of the short-lived lifetime component on excitation wavelength.

To further verify the omission of multiexciton effects, the average number of photons absorbed per nanocrystal ($\bar{N}$) was calculated[39]

$$\bar{N} = \frac{\sigma \lambda E}{hc} \tag{3}$$

where σ is the absorption cross section, λ is the excitation wavelength, E is the laser energy per cm^2, h is Planck's constant and c is the speed of light. From these calculations, it was found that the average number of photons absorbed per nanocrystal was less than 1 for excitation at both 20 nm above the band gap and at 400 nm.[40]

Figure 8a−d shows that there is both a size and compositional dependence on the electron−hole recombination of the nanocrystals. Focusing first on the size dependence, an increase in the nanocrystal diameter is accompanied by an increase in the short-lived component for band edge emission, τ_1. The short-lived component, τ_1, representing the lifetime of fluorescence decay at the band edge, is comprised of both a radiative decay from electron−hole recombination and a nonradiative decay via trap states. Upconversion observes only the radiative recombination, but the nonradiative process depletes the radiative state. We attribute the changes observed in the measured decay lifetime to the effect surface trapping has on electron−hole

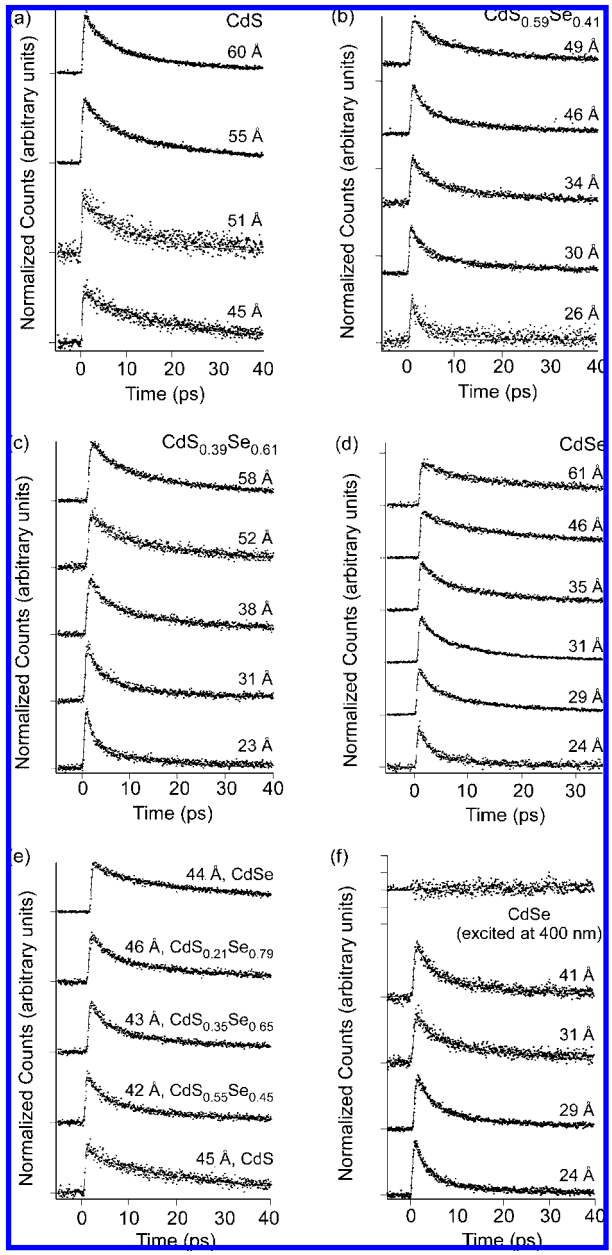

Figure 6. Fluorescence upconversion spectra (dots) with fits (solid lines) of (a) CdS nanocrystals (as the band edge absorption became too close to the excitation source, it was not possible to obtain upconversion data for smaller sizes of CdS), (b) $CdS_{0.59}Se_{0.41}$ alloy nanocrystals, (c) $CdS_{0.39}Se_{0.61}$ alloy nanocrystals, (d) CdSe nanocrystals excited 20 nm above the band edge, (e) 44 Å (±5%) nanocrystals of varying composition, and (f) CdSe nanocrystals excited at 400 nm (due to limitations of the laser dyes used for tuning the experiment, it was not possible to obtain upconversion data for larger sizes of CdSe while exciting at 400 nm). At the top of (f) is a representative residual plot for 41 Å CdSe nanocrystals.

recombination. As the size of the nanocrystal increases, the surface-to-volume ratio decreases, and there is a reduction in the overlap of the electron and hole wave functions.[41] This is coincident with a decreased wave function overlap with the nanocrystal surface, which leads to less surface trapping. Correspondingly, band edge recombination begins to dominate. This accounts for the increase in τ_1 with increase in nanocrystal size.

By further comparing the magnitude of τ_1 with changing nanocrystal composition, a definitive decrease in τ_1 is seen as the sulfur contribution increases (Figure 9). This behavior

TABLE 1: Calculated Amplitude Percentages for Nanocrystals of Varying Size and Composition[a]

diameter (Å)	% Amp 1	% Amp 1 error (±)	% Amp 2	% Amp 2 error (±)
CdSe (excited 20 nm above band edge)				
24	81.9	3.0	18.1	7.3
29	60.9	1.6	39.1	1.9
31	58.9	2.2	41.1	3.0
35	54.4	1.4	45.6	1.5
44	31.6	2.9	68.4	1.8
60	36.0	3.8	64.0	2.8
CdSe (excited at 400 nm)				
24	81.3	3.2	18.7	3.4
29	74.3	4.6	25.7	4.6
31	65.7	5.6	34.3	4.8
41	73.9	7.5	26.1	7.7
$CdS_{0.39}Se_{0.61}$				
23	75.9	2.3	24.1	2.8
31	74.4	2.2	25.6	4.2
38	58.8	2.9	41.2	3.9
52	50.4	5.1	49.6	5.4
58	52.2	2.8	47.8	2.9
$CdS_{0.59}Se_{0.41}$				
26	79.0	4.5	21.0	7.1
30	70.6	1.5	29.4	2.3
34	62.5	3.5	37.5	5.2
46	68.1	2.1	31.9	3.3
49	55.5	2.7	44.5	2.4
CdS				
45	28.5	8.2	71.5	4.3
51	53.9	13.7	46.1	9.6
55	44.3	2.6	55.7	2.0
60	57.6	2.9	42.4	3.0

[a] Corresponding amplitude percentages for τ_1 (short-lived decay) and τ_2 (long-lived decay) for CdSe, CdS and CdS_xSe_{1-x} nanocrystals from fitting of the ultrafast data. The negative amplitudes of the rise times are not incorporated into the calculation of percent composition, as we are focusing on the radiative and nonradiative contributions to the decay itself.

TABLE 2: Calculated Amplitude Percentages for 44 Å CdSe, CdS and CdS_xSe_{1-x} Alloy Nanocrystals[a]

composition (x)	diameter (Å)	% Amp_1	% Amp_2
1	45	28.6	71.4
0.55	42	59.8	40.2
0.35	43	62.6	37.4
0.21	46	58.9	41.1
0	44	31.6	68.4

[a] Corresponding amplitude percentages for τ_1 (short-lived decay) and τ_2 (long-lived decay) for 44 Å (±5%) nanocrystals spanning the compositional range from pure CdS ($x = 1$) to pure CdSe ($x = 0$).

indicates that carrier dynamics are not only size dependent but are indeed also composition dependent. A simple possibility might be that this behavior could be explained by electron−hole mobility due to the difference in the effective mass of the electron and hole in the individual materials. However, it is clear that this trend cannot simply be attributed to the difference in effective mass ($m_h{}^*_{CdS} = 0.7$ and $m_h{}^*_{CdSe} = 0.4$), as a larger effective mass equates to slower mobility, which is opposite of the trend seen here, as our data shows $\tau_{1CdSe} > \tau_{1CdS}$. It has been reported that nanocrystals synthesized with elemental sulfur have been found to have more surface defects, acting as traps on the nanocrystal surface.[42] Thus, it is plausible that by increasing the amount of sulfur present, the concentration of total surface trap states is being increased. Therefore, as the sulfur content increases, trapping should become more efficient

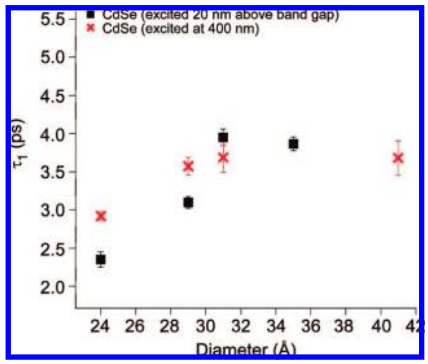

Figure 7. Graph of τ_1 versus nanocrystal diameter for CdSe nanocrystals excited at 20 nm above the band edge peak absorption and at 400 nm. There appears to be no substantial dependence of τ_1 on excitation wavelength.

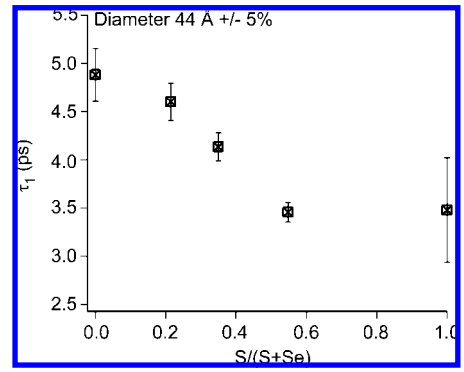

Figure 9. Graph of τ_1 versus nanocrystal composition for a series of 44 Å (±5%) nanocrystals. τ_1 is shown to decrease with increasing sulfur contribution, indicating a compositional dependence of the short-lived lifetime.

and the radiative recombination lifetime should decrease. This is consistent with our results, as we have found τ_1 decreases with increasing sulfur composition.

A size and compositional dependence of the long-lived time component (τ_2) can also be seen in Figures 10 and 11. For CdSe, the long-lived component for band edge emission has previously been attributed to relaxation from a triplet state to the ground state.[1] Due to experimental restrictions, the time scale for this component is not well determined, and even though the fit is on the order of tens of picoseconds, the lifetime of the triplet state is on the nanosecond time scale.[43] Even so, this effect is expected to be stronger for smaller nanocrystals,[44] as larger nanocrystals tend to recombine through the transition from the singlet to the ground state.[1] Thus, it is expected an increase in τ_2 and its amplitude (Table 1) should accompany an increase in nanocrystal size.[1] While this appears to be true for CdSe and, to a lesser extent, $CdS_{0.39}Se_{0.61}$, this trend is not seen in $CdS_{0.59}Se_{0.41}$ and CdS. With the addition of sulfur, τ_2 begins to decrease. This change in behavior could also be attributed to an increase in surface trapping caused by increased surface defects[42] for nanocrystal systems containing sulfur.

From the data presented here, it appears that with the addition of sulfur, surface trapping begins to dominate both the short- and long-lived nanocrystal lifetime components. Although it is not clear from the experimental data shown here whether such increased surface trapping can be entirely attributed to hole trapping, it should be noted that processes occurring on the order of 20−30 ps have been previously reported as electron trapping in CdS.[45]

In order to determine if this increase in surface trapping could be structure related, we proposed to use Z-STEM imaging to

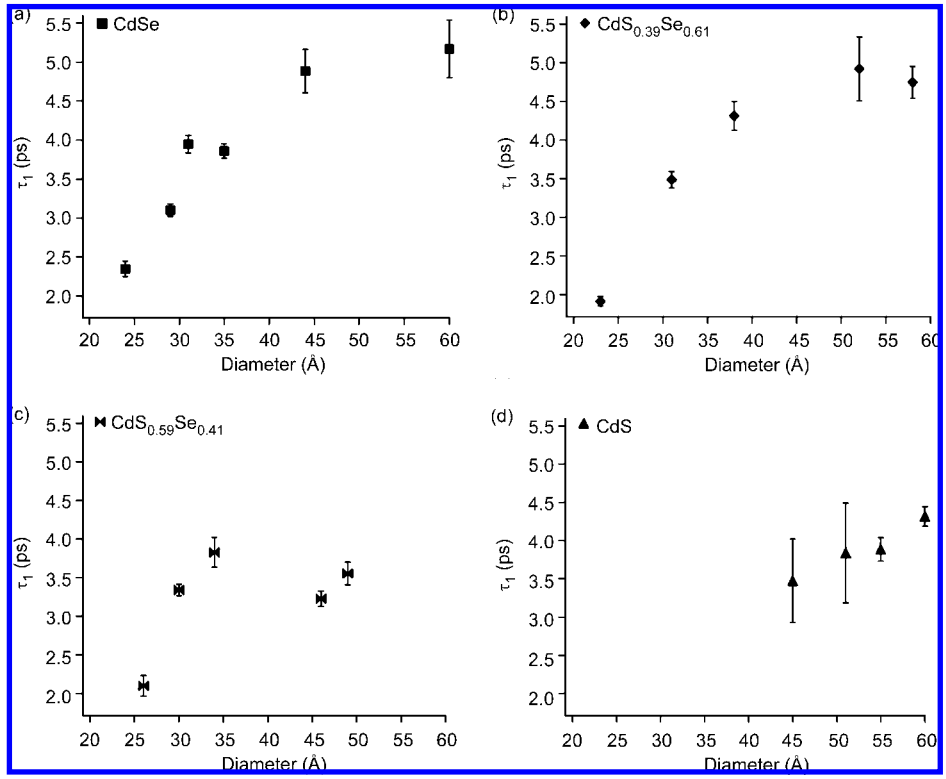

Figure 8. Graph of τ_1 versus nanocrystal diameter for (a) CdSe, (b) $CdS_{0.39}Se_{0.61}$, (c) $CdS_{0.59}Se_{0.41}$ and (d) CdS nanocrystals. The increase in τ_1 corresponds to the reduction in surface-to-volume ratio, resulting in a reduction in the overlap of the electron and hole wave functions with the nanocrystal surface. Not only is there a dependence of the short-lived lifetime on size, but there is also a composition dependence, as seen by the decrease in τ_1 as the sulfur contribution increases.

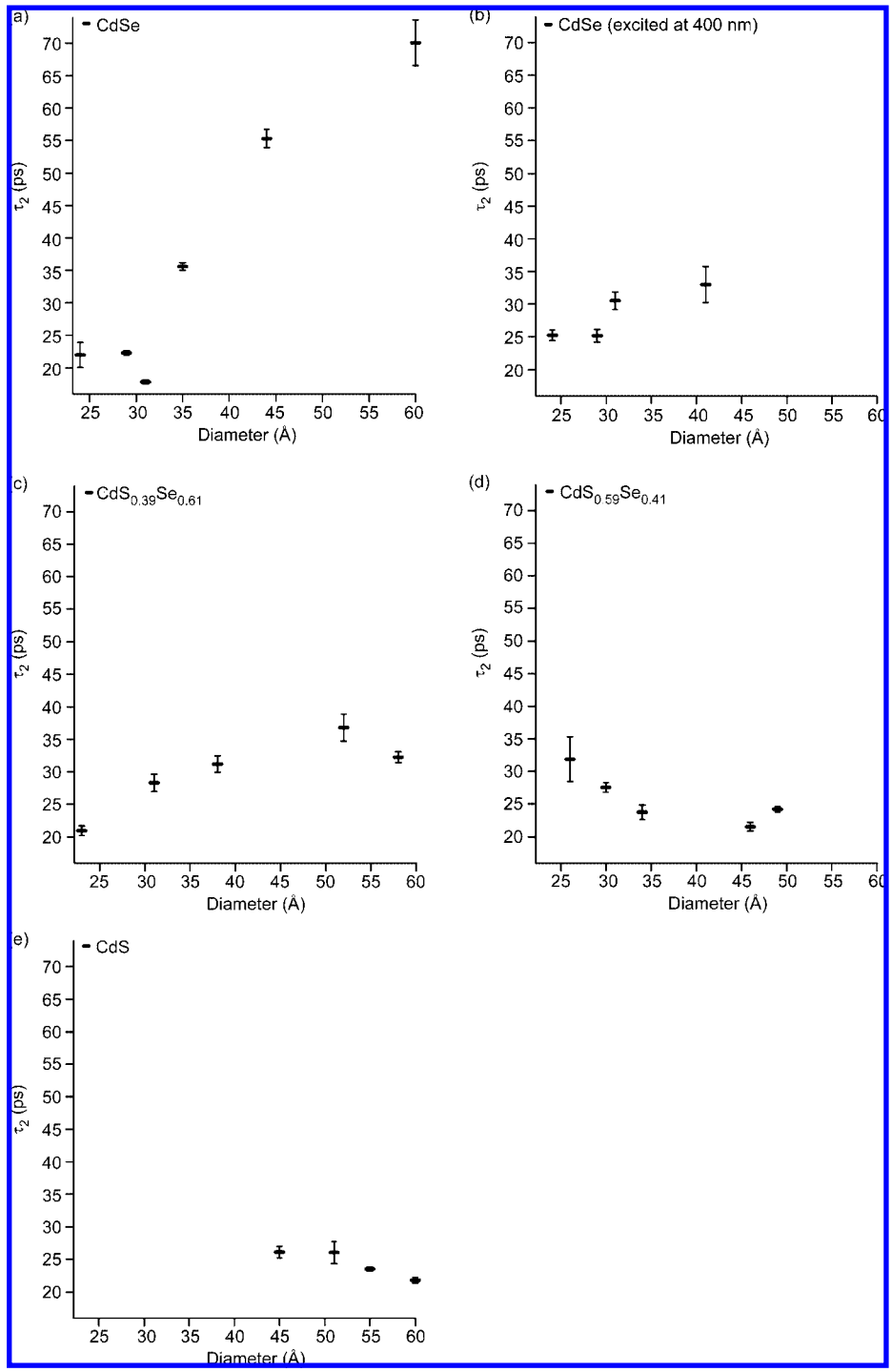

Figure 10. Graph of τ_2 versus nanocrystal diameter for (a) CdSe excited 20 nm above the band edge, (b) CdSe excited at 400 nm, (c) $CdS_{0.39}Se_{0.61}$, (d) $CdS_{0.59}Se_{0.41}$, and (e) CdS.

gain insight into both the structural ordering of the system and any defects present. We hypothesized that CdS has a higher degree of disorder (e.g., structural defects) than CdSe, and, therefore, increasing the contribution of sulfur to CdS_xSe_{1-x} alloy nanocrystals would increase the defects within the system, leading to a greater chance for nonradiative recombination and a shorter lifetime. This would not only agree with the trend for τ_1 seen in Figure 9, but would also be consistent with the previous hypothesis that a higher concentration of total surface trap states with the addition of sulfur contributes to a decrease in the radiative recombination lifetime. Thus, the structural order of the systems should be able to be used to predict the composition-dependent effect seen in the dynamics of the nanocrystals (Figures 8–11). Additionally, we proposed that defects, caused by the addition of sulfur, could be seen on the surface of the nanocrystals through Z-STEM imaging. It was expected that, with the addition of sulfur, degeneration of the surface would become apparent.

To test these ideas, we decided to use stacking faults as a measure of the degree of disorder in the nanocrystal systems and to look for defects on the nanocrystals as an indication of surface trapping. It should be mentioned that oleic acid CdSe nanocrystals have significantly more stacking faults than CdSe nanocrystals synthesized with tri-*n*-octylphoshine oxide (TOPO)

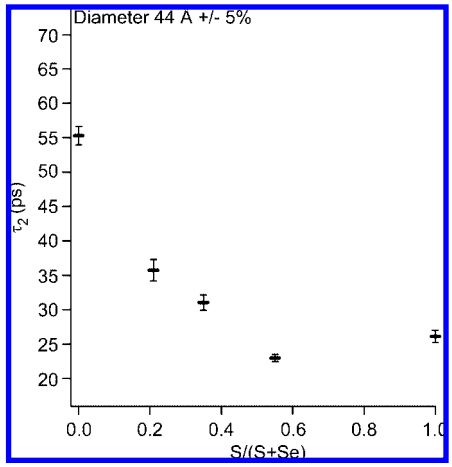

Figure 11. Graph of τ_2 versus nanocrystal composition for a series of 44 Å (±5%) alloy nanocrystals. It can be seen that τ_2 begins to decrease in the CdS_xSe_{1-x} alloy material. The decrease in τ_2 with increasing sulfur contribution is attributed to increased trapping at the nanocrystal surface.

and hexadecylamine (HDA).[35] As such, it would be expected that the radiative lifetimes for OA CdSe would be less than those for TOPO:HDA CdSe. Comparing our data with previously published results on TOPO:HDA CdSe nanocrystals,[46] it is found that τ_1 is shorter for OA CdSe at smaller nanocrystal sizes. However, focusing back on the alloy system, a trend in the degree of disorder for CdSe, $CdS_{0.50}Se_{0.50}$ and CdS is not clearly visible in the Z-STEM images (Figure 12). From these images, it is not apparent that there is an increased number of stacking faults, signifying a greater degree of disorder for oleic acid nanocrystal systems containing sulfur, as previously expected. Additionally, as seen in the Z-STEM images in Figure 12, surface degradation cannot be demonstrated due to oxidation of the nanocrystal surface caused by sample exposure to an intense light source that is used to reduce the amount of contamination experienced during Z-STEM imaging.

Although current attempts to use Z-STEM imaging to help elucidate the difference in the carrier dynamics among CdSe, CdS and CdS_xSe_{1-x} alloy nanocrystals based on the nanocrystal surface have not yet yielded constructive information, it is still believed that the compositional dependence on the short-lived (τ_1) and long-lived (τ_2) components of fluorescence lifetime at the band edge arise from increased surface trapping for nanocrystal systems containing sulfur. Changes in surface trapping could possibly be explained by a difference in chemical reactivity for the various nanocrystal systems. Specifically, the chemical reactivity of the structure can be looked at in terms of the HOMO−LUMO gap. In most cases, as LUMO energies decrease and HOMO energies increase, the reactivity increases.[47] Thus, softer chemical species, having smaller HOMO−LUMO gaps, are typically more reactive than harder species.[47] Hardness (η) is defined by the equation

$$\eta = \frac{1}{2}(I - A) \tag{4}$$

where I is ionization potential and A is electron affinity. Softness (σ) is expressed as the inverse of hardness

$$\sigma = \frac{1}{\eta} \tag{5}$$

Using eqs 4 and 5, the softness values of Se and S have been calculated and reported in Table 3. From these calculations, Se, having a larger σ value, should be more reactive.

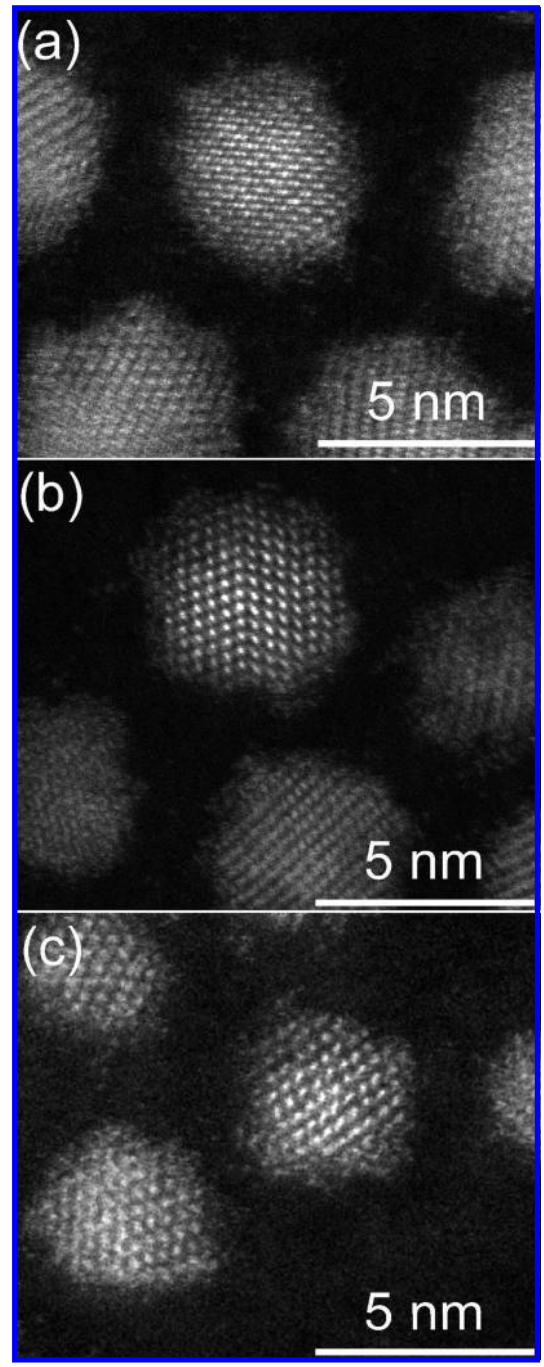

Figure 12. Z-STEM images of (a) CdSe, (b) $CdS_{0.50}Se_{0.50}$ and (c) CdS nanocrystals.

TABLE 3: Calculated Hardness and Softness Values for Se and S[a]

	I (eV)	A (eV)	η	σ
S	10.36001	2.077104	4.1415	0.2415
Se	9.75235	2.020670	3.8658	0.2587

[a] Ionization potential and electron affinity values were taken from the CRC Handbook of Chemistry and Physics.[48]

If we look at this reactivity in terms of dangling Se and S bonds on CdSe and CdS nanocrystals, Se should then be more likely to either bind to ligands or oxidize. In other words, fewer Se dangling bonds should be available for surface trapping. As the band gap of CdSe is smaller than that of CdS, CdSe should be more reactive than CdS. Thus, the CdSe nanocrystal surface is more likely to be oxidized or passivated than the CdS surface.

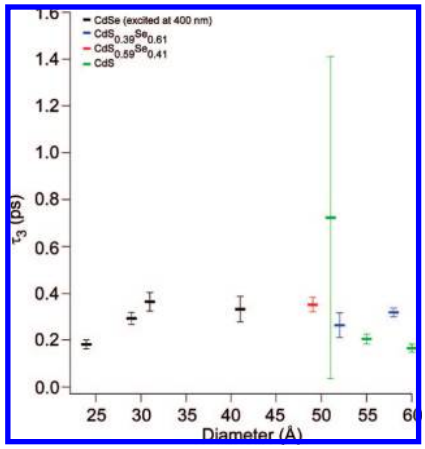

Figure 13. Graph of τ_3 versus nanocrystal diameter. There does not seem to be a substantial dependence of the risetime on size or composition. The exceptionally large error reported for the 51 Å CdS nanocrystal sample is attributed to the large amount of scatter in the data set.

This behavior is consistent with our results, as we have found that as the amount of sulfur increases, τ_1 decreases, indicating there are more trap states on the nanocrystal surface.

For several of the nanocrystal samples, a risetime (τ_3), representing intraband hole relaxation,[1] was also observed (Figure 13). Extremely small nanocrystals do not typically exhibit a risetime. For other samples, calculation of the risetime could not be achieved due to either the resolution of the experiment or scatter in the data resulting from the low signal-to-noise ratio. With both decrease in nanocrystal size and increase in alloy sulfur contribution the energy difference between the excitation wavelength and band edge absorbance decreases. As the excitation wavelength moves closer to the band edge, there is less thermal energy to dissipate. Thus, slightly shorter rise times would be expected for smaller sulfur-heavy nanocrystals. However, as seen in Figure 13, unlike the short- and long-lived decay components, there does not appear to be any significant dependence of risetime on size or composition, indicating that there is no apparent energy-dependence on the relaxation of the charge carriers to the emitting band edge state.

Conclusion

A compositional dependence of the Stokes shift has been observed for CdSe, CdS and CdS_xSe_{1-x} alloy nanocrystals. Not only is the Stokes shift found to nearly double for CdS_xSe_{1-x} alloy nanocrystals, but the Stokes shift also seems to reach a maximum value close to the middle of the compositional range. This behavior is attributed to the nonlinear effects of alloying.

The effect of surface trap states on band edge recombination in CdSe, CdS and CdS_xSe_{1-x} alloy nanocrystals has been determined using fluorescence upconversion spectroscopy. From the fluorescence upconversion data, it has been shown that there is both a size and composition dependence on the short-lived (τ_1) and long-lived (τ_2) components of fluorescence lifetime at the band edge. However, there appears to be no size or composition dependence on the reported rise times (τ_3).

The increase in τ_1 with nanocrystal size is explained by the decrease in accessible trap sites through a reduction in the surface-to-volume ratio, where the reduction in surface-to-volume ratio results in a reduction in the overlap of the electron and hole wave functions with the nanocrystal surface. With increasing sulfur content, a reduction in the magnitude of τ_1 is seen. This behavior is explained by an increase in total surface trap states associated with the addition of sulfur. Furthermore, τ_2 is seen to increase with increasing nanocrystal size for both CdSe and $CdS_{0.39}Se_{0.61}$. However, with increasing sulfur contribution, a reversal in the trend for τ_2 is observed. This change is also attributed to an increase in surface trapping with the addition of sulfur.

We proposed that Z-STEM imaging could be used to observe the structural disorder and surface defects believed to cause the compositional dependence on carrier recombination. While such analysis from the images was not possible, it is believed that further insight into the recombination dynamics of the varying compositional systems can be gained by looking at the band gap for CdSe and CdS in terms of chemical reactivity. The more reactive the surface, the more likely it is to be oxidized or passivated. This would result in fewer trap states and an increase the lifetime for τ_1.

The results reported here offer a detailed illustration of electron−hole recombination at the band edge of CdS_xSe_{1-x} alloy nanocrystals. These results reveal that the kinetics of the recombination dynamics of the nanocrystals are indeed dependent on variations in composition. By illuminating the impact that compositional modifications will have on carrier dynamics, these results help move the nanocrystal field one step closer to precision tunability of electron−hole pair dynamics, allowing these materials to be tailored for a variety of applications.

Acknowledgment. Funding for this work was provided by the U.S. Department of Energy (DEFG0202ER45957).

References and Notes

(1) Underwood, D. F.; Kippeny, T.; and Rosenthal, S. J. *J. Phys. Chem. B* **2001**, *105*, 436.
(2) Brus, L. *J. Phys. Chem.* **1986**, *90*, 2555.
(3) Alivisatos, A. P. *Science* **1996**, *271*, 933.
(4) Coe, S.; Woo, W.; Bawendi, M. G.; and Bulovic, V. *Nature* **2002**, *420*, 800.
(5) Huynh, W. U.; Dittmer, J. J.; Teclemariam, N.; Milliron, D. J.; Barnham, K. W. J.; and Alivisatos, A. P. *Phys. Rev. B* **2003**, *67*, 115326.
(6) Nozik, A. *J. Inorg. Chem.* **2005**, *44*, 6893.
(7) Bruchez, M.; Moronne, M.; Gin, P.; Weiss, S.and.; Alivisatos, A. P. *Science* **1998**, *281*, 2013.
(8) Rosenthal, S. J.; Tomlinson, I.; Adkins, E. M.; Schroeter, S.; Adams, S.; Swafford, L.; McBride, J.; Wang, Y. Q.; DeFelice, L. J.; and Blakely, R. D. *J. Am. Chem. Soc.* **2002**, *124*, 4586.
(9) Schreuder, M. A.; Gosnell, J. D.; Smith, N. J.; Weiss, S. M.; and Rosenthal, S. J. *J. Mater. Chem.* **2008**, *18*, 970.
(10) Bowers, M. J., II.; McBride, J. R.; and Rosenthal, S. J. *J. Am. Chem. Soc.* **2005**, *127*, 15378.
(11) Underwood, D. F.; Kippeny, T.and.; Rosenthal, S.; J, *Eur. Phys. J. D* **2001**, *16*, 241.
(12) Swafford, L. A.; Weigand, L. A.; Bowers, M. J., II.; McBride, J. R.; Rapaport, J. L.; Watt, T. L.; Dixit, S. K.; Feldman, L. C.; Rosenthal, S. J. *J. Am. Chem. Soc.* **2006**, *128*, 12299.
(13) Zimmer, J. P.; Kim, S.-W.; Ohnishi, S.; Tanaka, E.; Frangioni, J. V.; and Bawendi, M. G. *J. Am. Chem. Soc.* **2006**, *128*, 2526.
(14) Gadd, S. E. Excited State Carrier Dynamics in CdS_xSe_{1-x} Semiconductor Alloys as Studied by Ultrafast Fluorescence Spectroscopy, University of California, 1995.
(15) Hane, J. K.; Prisant, M. G.; Harris, C. B.; Meyer, G. J.; Leung, L. K.; Ellis, A. B. *J. Phys. Chem.* **1989**, *93*, 7975.
(16) Hane, J. K. The Picosecond Dynamics of Electron-Hole Pairs in Graded and Homogeneous CdS_xSe_{1-x} Semiconductors, University of California, 1995.
(17) Zhang, F. J.; Zhang, L. M.; and Claus, R. O. *Smart Mater. Struct.* **2007**, *16*, 243.
(18) Zhang, X.and.; Izutsu, M. *Jpn. J. Appl. Phys. Part 1* **1998**, *37*, 6025.
(19) Shen, Q.; Toyoda, T.; Hirose, Y.; Katayama, K.; Yui, H.; Fujinami, M.; Sawada, T.; and Harata, A. *Anal. Sci.* **2001**, *17*, s241.
(20) Toyoda, T.; and Shen, Q. *Anal. Sci.* **2001**, *17*, s259.
(21) Cruz, C. H. B.; Cesar, C. L.; Barbosa, L. C.; de Paula, A. M.and.; Tsuda, S. *Appl. Surf. Sci.* **1997**, *109/110*, 30.
(22) Qu, L.and.; Peng, X. *J. Am. Chem. Soc.* **2002**, *124*, 2049.

(23) Bhasikuttan, A. C.; Suzuki, M.; Nakashima, S.; and Okada, T. *J. Am. Chem. Soc.* **2002**, *124*, 8398.

(24) Kahlow, M. A.; Jarzeba, W.; DuBruil, T. P.; and Barbara, P. F. *Rev. Sci. Instrum.* **1988**, *59*, 1098.

(25) Morello, G.; Anni, M.; Cozzoli, P. D.; Manna, L.; Cingolani, R.; and De Giorgi, M. *J. Phys. Chem. C* **2007**, *111*, 10541.

(26) Kippeny, T. C.; Bowers, M. J., II.; Dukes, A. D., III.; McBride, J. R.; Orndorff, R. L.; Garrett, M. D.; and Rosenthal, S. J. *J. Chem. Phys.* **2008**, *128*, 084713.

(27) Efros, A. L.; Rosen, M.; Kuno, M.; Nirmal, M.; Norris, d. J.and.; Bawendi, M. *Phys. Rev. B* **1996**, *54*, 4843.

(28) Kuno, M.; Lee, J. K.; Dabbousi, B. O.; Mikulec, F. V.; Bawendi, M. G. *J. Chem. Phys.* **1997**, *106*, 9869.

(29) Murray, C. B.; Norris, D. J.; and Bawendi, M. G. *J. Am. Chem. Soc.* **1993**, *115*, 8706.

(30) Huang, Y. H.; Cheng, C. L.; Chen, T. T.; Chen, Y. F.; Tsen, K. T. *J. Appl. Phys.* **2007**, *101*, 103521.

(31) Kang, H. S.; Kim, J. W.; Kim, J. H.; Lee, S. Y.; Li, Y.; Lee, J.-S.; Lee, J. K.; Nastasi, M. A.; Crooker, S. A.; Jia, Q. X. *J. Appl. Phys.* **2006**, *99*, 066113.

(32) Bailey, R. E.and.; Nie, S. *J. Am. Chem. Soc.* **2003**, *125*, 7100.

(33) Wei, S. H.; Zhang, S. B.; Zunger, A. *J. Appl. Phys.* **2000**, *87*, 1304.

(34) Wu, J.; Walukiewicz, W.; Yu, K. M.; Ager, J. W., III.; Haller, E. E.; Lu, H.; Schaff, W. J. *Appl. Phys. Lett.* **2002**, *80*, 4741.

(35) McBride, J. R.; Kippeny, T. C.; Pennycook, S. J.; Rosenthal, S. J. *Nano Lett.* **2004**, *4*, 1279.

(36) McBride, J.; Treadway, J.; Feldman, L. C.; Pennycook, S. J.; Rosenthal, S. J. *Nano Lett.* **2006**, *6*, 1496.

(37) Ellingson, R. J.; Beard, M. C.; Johnson, J. C.; Yu, P.; Micic, O. I.; Nozik, A. J.; Shabaev, A.and.; Efros, A. L. *Nano Lett.* **2005**, *2005*, 865.

(38) Ellingson, R. J.; Blackburn, J. L.; Yu, P.; Rumbles, G.; Micic, O. I.; Nozik, A. J. *J. Phys. Chem. B* **2002**, *106*, 7758.

(39) Al Salman, A. Spectroscopy and Kinetic Studies of Electron-Hole Recombination in CdSe Nanoparticles: Effect of Size, Shape and Lattice Structure, ISIC Institut des sciences et ingénierie chimiques, 2007.

(40) Garrett, M. D. Band Edge Recombination in CdSe, CdS and CdS_xSe_{1-x} Alloy Nanocrystals Observed by Ultrafast Fluorescence Upconversion: The Effect of Surface Trap States Vanderbilt University, 2008.

(41) de Mello Donega, C.; Bode, M.; Meijerink, A. *Phys. Rev. B* **2006**, *74*, 085320.

(42) Yordanov, G. G.; Adachi, E.; Dushkin, C. D. *Colloids Surf., A* **2006**, *289*, 118.

(43) Wang, H.; de Mello Donega, C.; Meijerink, A.; Glasbeek, M. *J. Phys. Chem. B* **2006**, *110*, 733.

(44) Nirmal, M.; Norris, D. J.; Kuno, M.; Bawendi, M. G.; Efros, A. L.; Rosen, M. *Phys. Rev. Lett.* **1995**, *75*, 3728.

(45) Logunov, S.; Green, T.; Marguet, S.; El-Sayed, M. A. *J. Phys. Chem. A* **1998**, *102*, 5652.

(46) Garrett, M. D.; Bowers, M. J., II.; McBride, J. R.; Orndorff, R. L.; Pennycook, S. J.; Rosenthal, S. J. *J. Phys. Chem. C* **2008**, *112*, 436.

(47) Carey, F. A.; Sundberg, R. J. *Advanced Organic Chemistry Part A: Strucutre and Mechanisms*, 4th ed.; Kluwer Academic/Plenum Publishers: New York, 2000.

(48) CRC Handbook of Chemistry and Physics, 76th ed.; CRC Press, Inc., Boca Raton, 1995.

JP803708R